

Induced Förster resonance energy transfer by encapsulation of DNA-scaffold based probes inside a plant virus based protein cage

Mark V de Ruiter¹, Nico J Overeem¹ , Gaurav Singhal^{1,2}
and Jeroen J L M Cornelissen¹ 

¹ Laboratory of Biomolecular Nanotechnology, MESA+ Institute of Nanotechnology, University of Twente, P O Box 217, 7500 AE, Enschede, Netherlands

² Flinders Centre for Nanoscale Science and Technology, Flinders University, GPO Box 2100, Adelaide, SA 5001, Australia

E-mail: j.j.l.m.cornelissen@utwente.nl

Received 15 December 2017, revised 16 February 2018

Accepted for publication 7 March 2018

Published 11 April 2018




CrossMark

Abstract

Insight into the assembly and disassembly of viruses can play a crucial role in developing cures for viral diseases. Specialized fluorescent probes can benefit the study of interactions within viruses, especially during cell studies. In this work, we developed a strategy based on Förster resonance energy transfer (FRET) to study the assembly of viruses without labeling the exterior of viruses. Instead, we exploit their encapsulation of nucleic cargo, using three different fluorescent ATTO dyes linked to single-stranded DNA oligomers, which are hybridised to a longer DNA strand. FRET is induced upon assembly of the cowpea chlorotic mottle virus, which forms monodisperse icosahedral particles of about 22 nm, thereby increasing the FRET efficiency by a factor of 8. Additionally, encapsulation of the dyes in virus-like particles induces a two-step FRET. When the formed constructs are disassembled, this FRET signal is fully reduced to the value before encapsulation. This reversible behavior makes the system a good probe for studying viral assembly and disassembly. It, furthermore, shows that multi-component supramolecular materials are stabilized in the confinement of a protein cage.

Keywords: viruses, fluorescent cascade, viral genome, self-assembly, fluorescent probes

 Supplementary material for this article is available [online](#)

(Some figures may appear in colour only in the online journal)

Introduction

Förster resonance energy transfer (FRET) is a well-studied phenomenon that occurs when two or multiple fluorescent dyes are in close proximity to one another. It is often employed to study binding interactions or separation distances of two compounds or proteins, but also as a probe to study, for example, enzymatic digestion processes [1–3]. Furthermore, the resulting increase in Stokes shift of the fluorescent emission can make FRET pairs more sensitive for detection than just a single dye in imaging in cells because there is less background fluorescence [4]. A one step FRET, in combination with DNA hybridisation is often studied because of the precise control

over the positioning of the dyes that can be obtained when using DNA base pairing. Recently, more elaborate structures of a two-step, multiple steps or even more complex dye systems have been evaluated [5, 6]. Multiple dyes arranged along a strand (of DNA) can be used for sequential energy transfer of photonic energy along increased distances and are referred to as photonic wires, which can be used for a device's optical function or as a readout in sensor-based applications [7].

In this contribution, we use a DNA-based FRET system to study the characteristics of virus protein assembly. In particular, the disassembly and assembly of viruses require more fundamental insight, to help better understand viruses and consequently help to treat diseases with a viral origin. FRET

has already been employed before to study disassembly of viruses *in vitro* [8–10]. This involved, however, mainly exterior modification of viruses with dyes or large fluorescent proteins, which can influence the viral assembly and stability in solution, as well as their uptake in cells [11]. It is, therefore, preferable to harness the interior. Especially the native nucleic acid cargo is an optimal candidate. Since DNA-based FRET systems consist for the most part of nucleic acids, it is a good place to start and use them as probes.

To test the feasibility of our system the cowpea chlorotic mottle virus (CCMV) is used. This is a plant virus, which can be disassembled at neutral pH and high salt concentrations (>0.3 M). Using calcium, the native RNA can be precipitated and separated from the free capsid proteins (CPs) [12]. The CPs have been shown to assemble back to their native structure of 28 nm diameter, with $T = 3$ Caspar and Klug icosahedral symmetry, under acidic conditions ($\text{pH} < 6.5$), in the presence of sufficient salt to shield the original RNA binding domains [13, 14]. These binding domains are formed by a number of positive charges near the N-terminus of the proteins. Alternatively, the CPs of the virus can assemble at neutral pH around many different negatively charged templates, where the assembly is triggered by modulating the ionic strength [15, 16]. This can result in various different shapes of virus-like particles (VLPs), having $T = 1$, $T = 2$, or $T = 3$ icosahedral symmetry, but also rods and other structures [17–20]. The CCMV virus is especially interesting because it is protein cage often used as a model system to study the assembly and disassembly of viruses [21].

This templating effect of negative charges is employed to encapsulated synthetic DNA-based photonic wires in the virus capsid, with the goal of using it as a probe for protein assembly, disassembly and determination of the interior spacing of the formed virus-like particle. Here, a photonic wire is constructed using three different dyes: ATTO 448, 565 and 647N, which have sufficient overlapping emission and extinction spectra for FRET experiments. These dyes are attached to three different single-stranded DNAs (ssDNA) of 35 nucleotides (nt). 30 nt of these ssDNA strands are orthogonally complementary to three different positions on a 120 nt templating strand of ssDNA. The dyes are sufficiently spaced to have minimal FRET energy transfer before encapsulation, but it is expected to have FRET after encapsulation. To enhance the formation of icosahedral virus-like particles, ssDNA nts are placed between the double stranded parts, leading to a more flexible chain due to their lower persistence length [22, 23]. Different combinations are evaluated with only two dyes on the templating strand, but also with all three different dyes attached to the templating strand. The 488, 565 and 647N positions and dyes are denoted in this work as dyes 1, 2 and 3 respectively (see also figure 1 for a description of the system). Clearly, the ssDNA strands can be designed such that these are complementary to the native genetic material of viruses, making this method viable for other viruses as well. Furthermore, this system is designed such, that it could also be used for different applications, for example to impose stoichiometric control over the encapsulation of multiple different cargo molecules inside a viral capsid [24].

Method

Unless specified otherwise, all compounds were purchased from Sigma-Aldrich, and all buffers were prepared with $18 \text{ M}\Omega \cdot \text{cm}$ MilliQ (Millipore) water.

DNA hybridisation

DNA with and without dyes was synthesized by Eurofins and dissolved in water at $200 \mu\text{M}$ before use. The three different DNA-dye-tags ($5'$ -AAA AAT GCA AGG CAG ATT CAC CGA CTG GAT CAA TT-3', $5'$ -AAA AAG GCC GTG ACC TAT TGC TAC GAC TGC TAT TC-3' and $5'$ -AAA AAA GCT CCA CCG ACT TTA CGA CGC CAA TTT GC-3'), modified at the $5'$ with ATTO 488, 565 and 647N dyes (ATTO-TEC) respectively, were hybridised with the 120 nt ssDNA templating strand ($5'$ -AAT TGA TCC AGT CGG TGA ATC TGC CTT GCA GAG AGG GAA GAA GAG GAA TAG CAG TCG TAG CAA TAG GTC ACG GCC AAG AAG GAG GGA AGA GCA AAT TGG CGT CGT AAA GTC GGT GGA GCT-3') in 2:2:2:1 ratio in Tris-HCl buffer pH 8 with 5 mM MgCl_2 and 0.1% SDS overnight. After the incubation, the resulting DNA-hybrids were purified using agarose gel electrophoresis with a 1.5% gel run for 2.5 h at 100 V, stained with SYBRsafe. The gel was imaged on a visi-blue transilluminator (UVP). It was possible to separate the newly formed hybrid from the ssDNA templating strand due to the different rate of migration of ssDNA and double-stranded DNA (dsDNA) [25]. The desired bands were cut from the gel and purified using 'Wizard SV gel and PCR clean-up system' (Promega). The purified DNA was eluted in MilliQ. Alternatively, size exclusion chromatography (FPLC) with a superpose 6/300 column on an Akta purifier (GE Healthcare) was used to analyse and separate the unbound DNA-dye-tags from the fully formed DNA hybrid. The samples were analysed using UV-vis to determine the concentration, DNA/dye and dye/dye ratios using the Lambert-Beer law. The ATTO 488, ATTO 565 and ATTO 647N extinction coefficients: $\epsilon = 9.0 \times 10^4$, 1.2×10^5 , $1.5 \times 10^5 \text{ M}^{-1} \text{ cm}^{-1}$ and correction factors at $\lambda = 260 \text{ nm}$ of 0.22, 0.27 and 0.04 were used for the calculations respectively. For DNA, the extinction coefficient was calculated [26] assuming the number of ssDNA and dsDNA nucleotides in the resulting DNA hybrid, for example the DNA-hybrid with all three dyes has 45 nt and 90 bp.

Production of CCMV CPs

CCMV was produced in black eyed pea plants according to the method developed by Verduin and adapted by Comellas Aragonès [27, 28]. In short: 10 d after planting the beans the cowpea plants were infected with the virus, followed by another 10 d of growth. The leaves were harvested without the stems, crushed and mixed with a pH 4.8 buffer containing 0.2 M sodium acetate, 10 mM ascorbic acid, 10 mM disodium EDTA, followed by filtration using a cheese-cloth, centrifugation and again filtration. Then PEG-6000 precipitation was applied. The virus was reconstituted in pH 5 acetate buffer and subjected to 16 h ultracentrifuge step

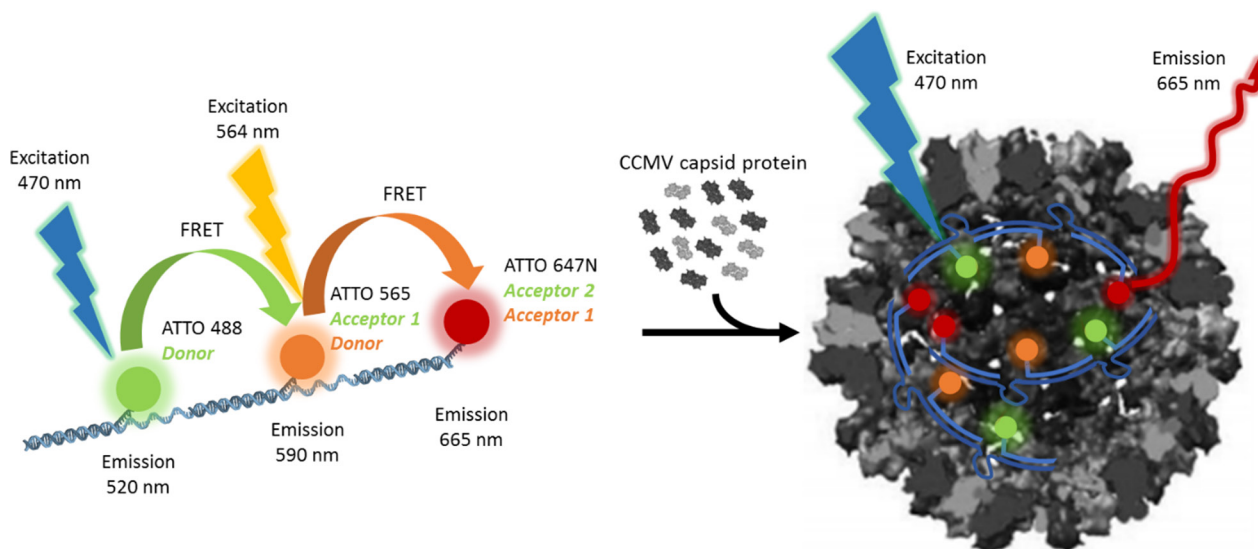


Figure 1. Schematic representation of the three different dyes connected to DNA, hybridised with a 120 nt templating strand (blue) on separate binding sites. ATTO 488 resides on position 1, ATTO 565 on position 2 and ATTO 647 at position 3, in green, orange and red, respectively. When the DNA-dye construct is mixed with CPs (in gray), these assemble into virus-like particles.

in 33% (w/w) CsCl at 10 °C and 255 000 rcf in a Sorvall WX80 ultracentrifuge. Successful virus formation was verified using size exclusion chromatography on a superpose 6/300 column, UV-vis absorbance and SDS-page using Mini-PROTEAN® TGX Stain-Free™ Precast Gels. The virus was dialysed from virus buffer (0.1 M sodium acetate, 1 mM disodium EDTA, 1 mM sodium azide, buffered at pH 5.0) to RNA isolation buffer (50 mM Tris, 0.5 M CaCl₂, 1 mM DTT, buffered at pH 7.5). The viral RNA was precipitated and pelleted by overnight centrifugation at 14 100 rcf. The supernatant containing the dimer of the CPs was dialysed to 5× assembly buffer (250 mM Tris, 250 mM NaCl, 50 mM KCl, 25 mM MgCl₂, pH 7.2). Successful removal of the RNA was confirmed by a 280/260 ratio above 1.55 and concentration of CP was determined using a 280 nm extinction coefficient of 24 075 M⁻¹ cm⁻¹.

Assembly studies

Assembly was induced by lowering the salt concentration in the presence of DNA. The capsid protein in 5× buffer was mixed in a 4:1 (v/v) ratio with the DNA in MilliQ. The respective solutions were diluted to achieve a final mass ratio of CP/DNA of 6, which is considered the optimum ratio for RNA encapsulation [29]. This resulted in a 1× assembly buffer (50 mM Tris, 50 mM NaCl, 10 mM KCl, 5 mM MgCl₂, pH 7.2), which was determined to be optimal for capsid assembly around nucleic acids. The assembly mixtures were incubated overnight at 4 °C. Native agarose gel electrophoresis stained with SYBR-safe DNA stain was used to show the reduced migration of the DNA in the gel and thus formation of virus-like particles. The gels were subsequently stained overnight with colloidal Coomassie stain (Biorad), followed by overnight destaining in MilliQ. The gels were analysed on a gel-doc EZ imaging system (Biorad). The assembled particles were purified using FPLC with the 1× assembly buffer, on a superpose 6 column,

or alternatively in 100 kDa MWCO spin filters (Millipore) at 4000 rcf, refreshing the buffer four times to remove unbound CP and DNA. The size distribution of the VLPs was measured with dynamic light scattering (DLS) in a Microtrac Nanotrak Wave W3043. The viscosity and refractive index of the buffer were assumed to be identical to water, and for VLPs the refractive index of $\eta = 1.54$ is used. Furthermore, the VLPs were imaged with transmission electron microscopy (TEM) on an FEG-TEM (Phillips CM 30) operated at 300 kV acceleration voltages. Samples were prepared on formvar Carbon 200 copper grids by incubating the samples for 1 min, draining the liquid, followed by 1% uranyl acetate staining for 15 s. The diameter of imaged particles was measured with ImageJ to determine the size distribution. Each particle was measured in two orthogonal directions. Concentrations and the ratios of the different dyes on the templating DNA strand were determined using a PerkinElmer Lambda 850 UV/vis spectrometer and a Nanodrop 1000 (Thermo Scientific).

Fluorescence studies

The fluorescence of the separate ATTO 488, 565 and 647N dye tags, different DNA-dye hybrids and DNA-dye hybrid VLPs were studied on a PerkinElmer LS55 fluorescence spectrometer, all using the same concentrations and filter settings. For the FRET measurements, excitation wavelengths of $\lambda = 470$ and 564 nm were used, having optimal excitation of the donor with minimal direct excitation of the acceptor(s). The graphs are from normalized data at maximum emission. From the original sensitised data, with at least three repeats, the area under the curve of the emission for the different dyes was determined using Origin software after subtraction of the background, direct excitation and contribution of the donor(s). Results were corrected for slight differences in concentrations. FRET efficiencies were calculated using the same method as previously applied on photonic wires [6]. Formula (1) is used to

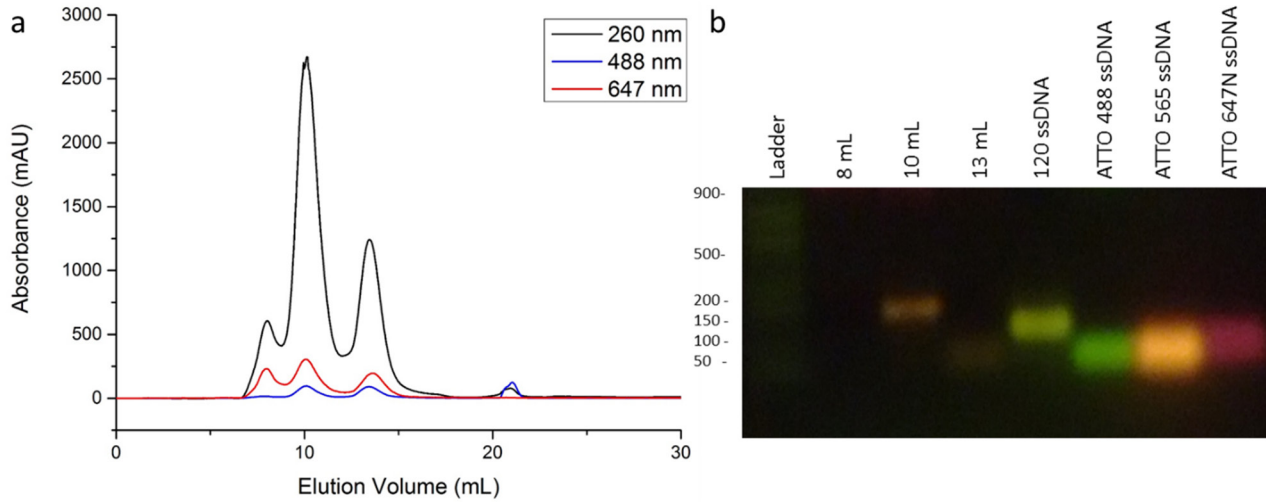


Figure 2. (a) Size exclusion chromatogram of the purification of the DNA hybrid with the ATTO 488, 565 and 647 N dyes attached. (b) Agarose gel electrophoresis analysis of the different elution peaks from the chromatogram. The 120 well is the templating strand and the 488, 565 and 647 well are the different ATTO dyes attached to 35 nt DNA strands.

calculate the energy transfer efficiency, and the corresponding separation distances of the dyes were calculated using formula (2). The overall efficiency for the two-step FRET was verified using formula (3), which includes the direct transfer from the first to the third dye and the signal resulting from the consecutive transfer past the second dye [30]. Where E is the FRET efficiency, with the subscript denoting which dye pair is specified; r represents donor-to-acceptor separation distance; R_0 is the Förster distance of the donor and acceptor pair, for which the refractive index of water and a random orientation factor were assumed; R_0 values of 63 Å for 1 + 2, 49 Å for 1 + 3 and 69 Å for the 2 + 3 dye FRET pairs are used. Φ_{AD} is the area of the terminal acceptor fluorescence in the presence of donor(s); Φ_A is the area of the same terminal acceptor in the absence of donor(s); Φ_D is the area of the donor in the absence of acceptor(s); and $Q_{D/A}$ are the respective quantum yields for the terminal acceptor and donor. Quantum yields of 80% for ATTO 488, 90% for ATTO 565 and 65% for ATTO 647N were used.

$$E = \left(\frac{\Phi_{AD} - \Phi_A}{Q_A} \right) / (\Phi_D / Q_D) \quad (1)$$

$$E = \frac{1}{1 + \left(\frac{r}{R_0} \right)^6} \quad (2)$$

$$E_{1-3 \text{ total}} = E_{1-2} * E_{2-3} + E_{1-3}. \quad (3)$$

Results and discussion

DNA assembly and purification.

The 35 nt ssDNA-dye hybrids were mixed in excess with the 120 nt template strand and incubated overnight to form the different constructs. The resulting DNA hybrids were purified using size exclusion chromatography (figure 2(a)) and agarose gel electrophoresis (figures 2(b) and supplementary figure SI 3 (stacks.iop.org/JPhysCM/30/184002/

[mmedia](#))). As a representative example from the 1 + 2 + 3 DNA-dye hybrid, the chromatogram shows a main peak around $V = 10$ ml elution volume. This peak is the DNA-dye hybrid with $\lambda = 260$ nm, 488 nm, 647 nm absorbance coming from the DNA, ATTO 488 and ATTO 647N respectively. The second main peak around $V = 13.5$ ml is most likely a mixture of the unbound 35 nt DNA with dyes, as it elutes at a larger volume. The ratio between the 260 and 488/647 absorbances indicates a lower amount of DNA per dye than in the $V = 10$ ml peak. $V = 21$ ml is most likely an impurity of unbound ATTO 488 dye. The formation of the DNA-dye hybrid is also confirmed on an agarose gel (figure 2(b)). Here the band of the $V = 13.5$ ml fraction runs as found at the same position as the bands of the different 35 nt dyes. Also, note that the newly formed DNA-dye-hybrid runs higher than the 120 nt template strand. This is caused by the formation of dsDNA; ssDNA runs 10% faster on a gel compared to dsDNA of the same length [25]. Also, the color on the gel confirms the presence of the dyes. The products were further characterized using UV-vis absorbance measurements, of which the results are summarized in supplementary figure SI 4. As expected, each hybrid has on average one of each dye per strand and the ratios of the different dyes on the different DNA-hybrids is around 1:1.

Formation of VLPs

As a starting point to confirm encapsulation and screen different assembly conditions, a native agarose gel electrophoresis was performed using the same concentrations of DNA-hybrid, capsid protein and unpurified assemblies of DNA-hybrid VLPs. Initially, DNA staining is applied, followed by overnight protein staining on the gel (supplementary figure SI 5). From this gel, it is clear that the encapsulated samples migrate different compared to the unencapsulated materials.

To purify the formed VLPs, size exclusion chromatography using an FPLC system was applied (figure 3(a)). The

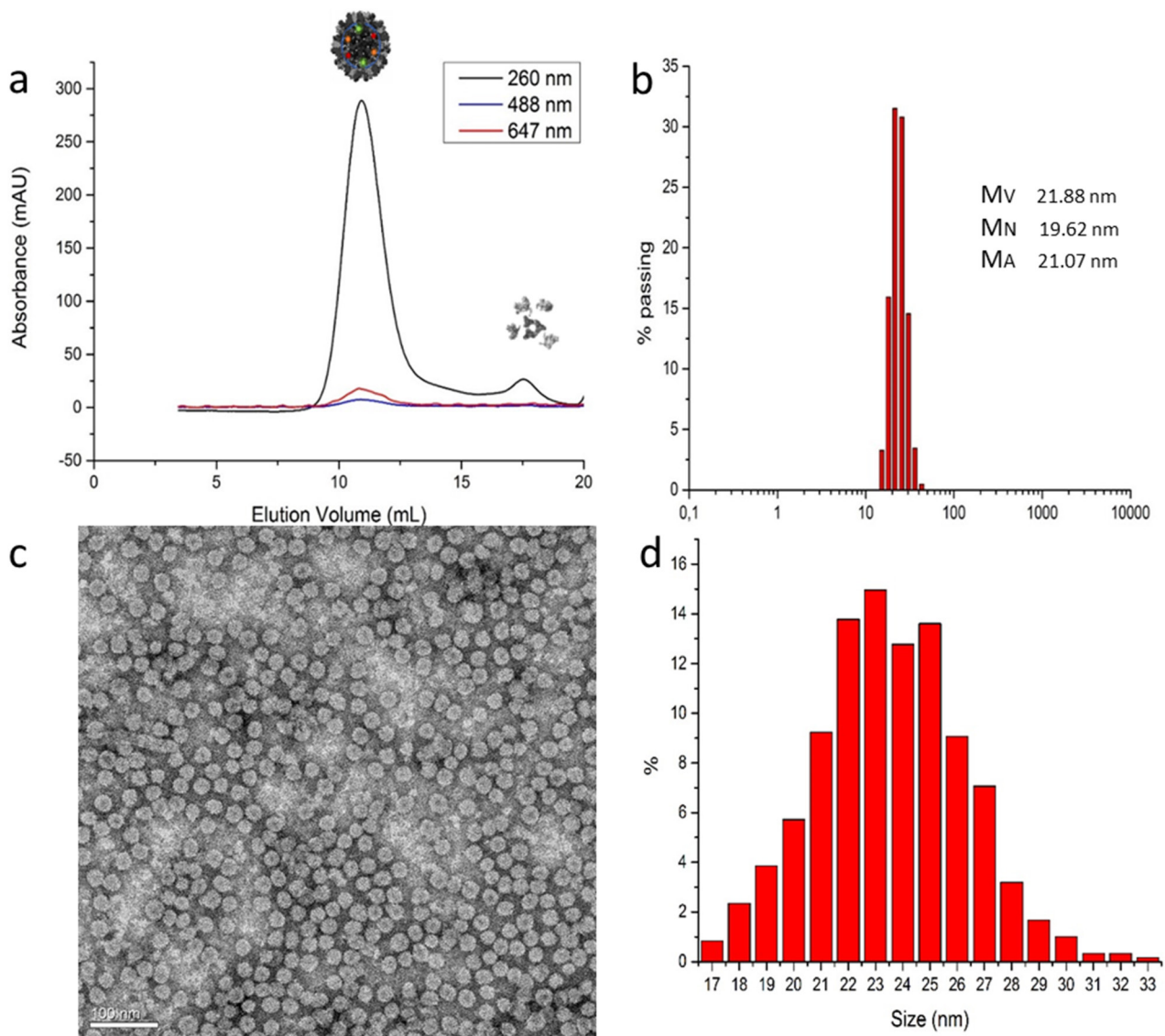


Figure 3. (a) FPLC chromatogram of the 1 + 2 + 3 DNA encapsulated in VLPs. (b) Size distribution and average sizes of VLPs in dynamic light scattering. (c) Representative TEM image of negatively stained VLPs. Scale bar is 100 nm. (d) Size analysis from the TEM, average particle size is 23.5 ± 2.2 nm.

$V = 11$ ml elution peak corresponds to larger assemblies, corresponding to the elution volume of the native virus. Likely, these are the VLPs filled with the DNA hybrids as indicated by the high $\lambda = 260$ nm absorbance and the co-elution of the different dyes. The $V = 18$ ml peak has a low $\lambda = 260$ nm absorbance and corresponds to the elution of the capsid protein dimers. There is virtually no DNA visible, presumably, all of the DNA hybrids are encapsulated. The $V = 11$ ml fractions were collected and analyzed using DLS (figure 3(b)). They contain particles with an area average diameter of $D \pm 21$ nm. Subsequent TEM (figures 3(c) and (d)) shows particles with $D = 23.5 \pm 2.2$ nm and confirms that these are spherical, as expected for icosahedral VLPs. The size corresponds to the range of $D = 20$ – 24 nm found for pseudo $T = 2$ or possibly swollen $T = 1$ particles with Caspar and Klug symmetry for CCMVs [24, 31]. Under the applied conditions, the CPs do not assemble into spherical capsids, but incidentally some

rods form [32]. This morphology we also observed for less than 1 in 500 particles in some of our samples (supplementary figure SI 6). SDS-PAGE on the purified VLPs eluting at $V = 11$ ml from the FPLC confirmed the presence of CP (supplementary figure SI 7).

Fluorescence analysis

To evaluate the effect of encapsulation on the fluorescent energy transfer, fluorescent emission scans were performed with $\lambda_{\text{ex}} = 470$ nm and 564 nm. The emission spectra, normalized to maximal fluorescence are shown in figure 4. It is clear that the fluorescence emission of the second (ATTO 565) and third dye (ATTO 647N) are increased with respect to the first dye (ATTO 488), upon encapsulation of the different DNA constructs in VLPs. For the one-step FRET systems, there is an increase in the emission of the second (ATTO

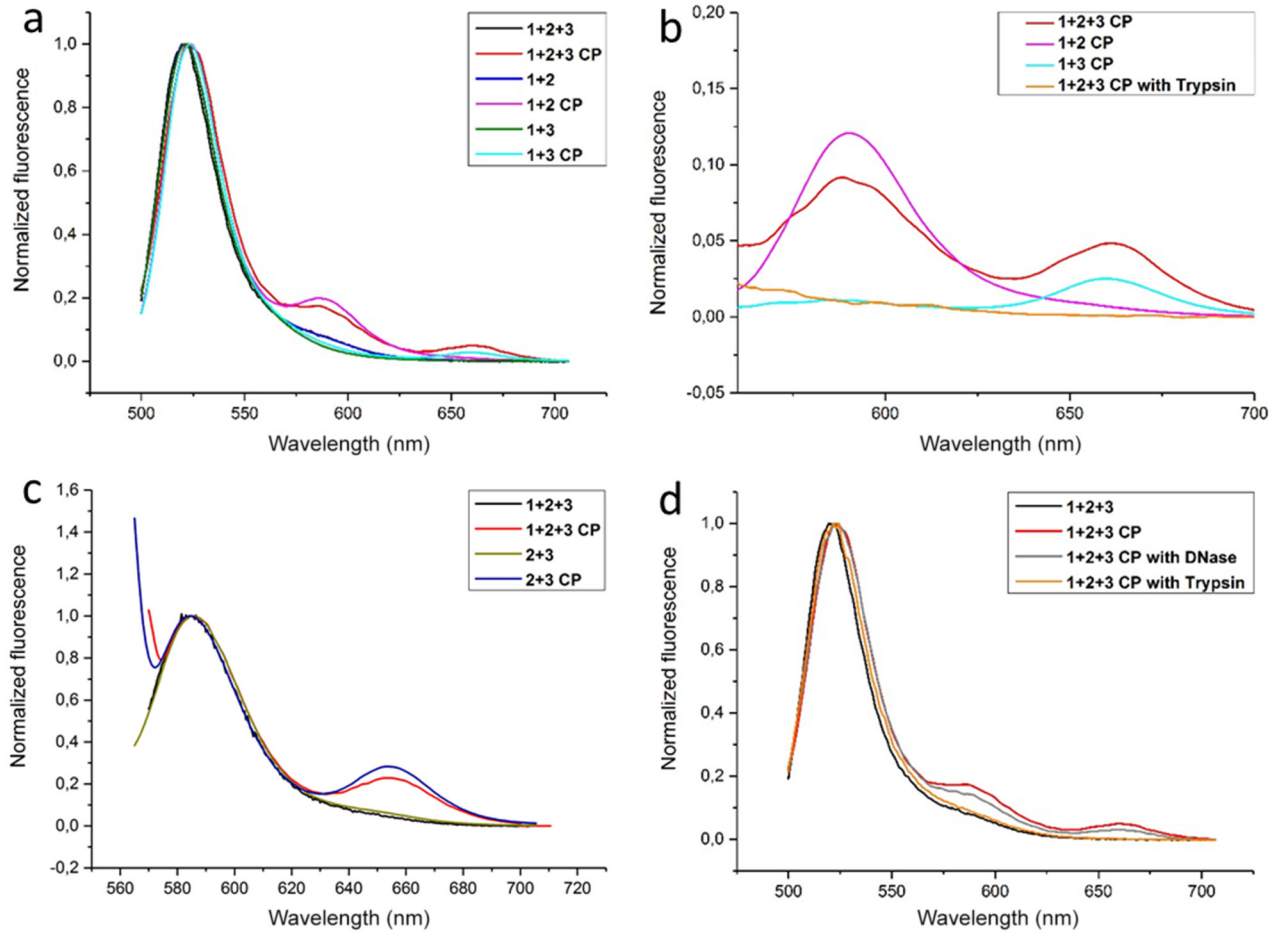


Figure 4. Fluorescence emission spectra of the DNA-hybrid constructs with different dye combinations before and after encapsulation (with CP), normalized to the maximum emission. (a) Excited at $\lambda = 470$ nm, (b) zoom of emission of non-encapsulated samples subtracted from the encapsulated samples, (c) excited at $\lambda = 564$ nm, (d) encapsulated samples digested with trypsin or DNase excited at $\lambda = 470$ nm.

565) dye around $\lambda_{em} = 590$ when the first dye is excited (figures 4(a) and (b)). The same holds for when the second dye is excited (figure 4(c)) and there is an increase in fluorescence around $\lambda_{em} = 664$ nm of the third (ATTO 647N) dye. Finally, increased emission of the third dye is observed when the first dye is excited. Formula (1), which holds for multi-FRET systems [6], was used for analysis to extract the FRET efficiencies (E) and separation distances of dyes are calculated using (2), the results are summarized in table 1 This showed an average increase in FRET efficiency by a factor of 7.9 for a one-step FRET. For the two-step FRET system (1 + 2 + 3), both for the second and third dye an increase of the fluorescence upon encapsulation in the VLP is observed. The fluorescence of the second dye is slightly lower (9.3) compared to the 1 + 2 system (9.7), which is likely the result of the relay energy transfer to the third dye. Consequently, the signal of the third dye is increased compared to the 1 + 3 system (from a factor of 8.9 to 16.4), because of the extra FRET contribution from the relay, which is shown in the literature to increase the FRET distance [30, 33].

Using the refractive index of water and a random orientation of the dyes, the average distance between the dyes is calculated. Dyes separated by one rigid and one flexible linker go from 11.7 nm for the free dye system to 9.0 ± 0.3 nm for

the encapsulated system. While the separation of dye 1 to dye 3, with two rigid and two flexible chains is decreased during encapsulation from 16.5 to 11.4 nm. To confirm if these results fit with theoretical calculations for the unencapsulated DNA hybrids the end to end distance was calculated, which is assumed similar to the average dye-dye distance. The dsDNA is assumed rigid [22] and has a length of 3.32 \AA bp^{-1} [34]. The 5 nt linker to the DNA is 6.76 \AA nt^{-1} [35], together with the literature persistence length [23] was used as input for formula (4). The length of the 15 nt flexible linker depends on the salt concentration, for which the experimental value of 5.3 nm from literature was used [36]. The dyes are attached to the DNA with C6 linkers and the resulting end to end distance was again calculated using formula (4) with literature data [37]. These values were taken as input for equation (5), which gave a radius of 12.1 nm for the direct neighbor separation (1 + 2 and 2 + 3 dyes) and 16.5 nm for the 1 + 3 dye pair, which is close to the spacings found experimentally.

$$R_F^2 = 2L_p[L_c + L_p (e^{-L_c/L_p} - 1)] \quad (4)$$

$$R_F^2 = \sum \langle (r_i - r_j)^2 \rangle. \quad (5)$$

Table 1. Calculated FRET efficiencies (E) and dye spacings from fluorescent data using formulas (1) and (2).

	DNA-hybrid	Efficiency 1 step	Efficiency 2 step	Spacing (Å)
$\lambda_{\text{ex}} = 470$ nm	1 + 2	0.0137		128
	1 + 2 CP	0.133		86.0
	1 + 3	0.003 10		164
	1 + 3 CP	0.0276		114
	1 + 2 + 3	0.0121	0.0033	131
	1 + 2 + 3 CP	0.113	0.0540	89.0
$\lambda_{\text{ex}} = 564$ nm	2 + 3	0.0427		122
	2 + 3 CP	0.141		92.5
	1 + 2 + 3	0.0204		132
	1 + 2 + 3 CP	0.168		90.0

Here L_p the persistence length of the DNA polymer, $r_i - r_j$ the separation of the subunits and L_c the contour length of the polymer segment.

The most probable explanation for the decreased separations in the encapsulated system is that the negatively charged DNA has an interaction with the positively charged arginine-rich motifs (ARMs) on the N-terminus of the CPs, which are also found in other viruses [38]. Some of the CPs can spontaneously lose this ARM, but an intact protein is needed for the initial DNA-CP binding. This leads to the (cooperative) formation of the VLP by bringing CPs in close proximity of each other [39]. In the formed capsids, the DNA is confined and presumably the degrees of freedom of the DNA are restricted in this way. Because of the net positive charge of the dyes, it is likely that these point inwards into the cavity of the VLPs due to charge repulsion by the positively charged CPs, additionally increasing the FRET efficiency. Literature suggests that the increase in FRET efficiency can be calculated using formula (3) [30], which gives $E = 0.046$ for our data, but the resulting efficiency for the two-step FRET is 17% higher. This increase in multiple step FRET efficiency in the capsid, and likely also for the one step FRET, can be explained by an antenna effect [5], as the virus likely encapsulates between two to three DNA-hybrid strands. This availability of multiple FRET routes results in higher efficiencies. The presence of multiple DNA strands per VLP can be explained by charge compensation between the ARMs and DNA [29].

To confirm that this system is useful for disassembly studies and that the increase in FRET efficiency is a consequence from the encapsulation of the DNA-dye-hybrid inside the VLPs, the encapsulated system was digested with trypsin. This enzyme degrades the capsid proteins resulting in the release of the DNA-dye-hybrid from the confinement of the VLP. The fluorescence emission spectrum of the trypsin digested sample is similar to that of the unencapsulated system (figures 4(b) and (d)), confirming that the increase in fluorescence is originating from the formation of VLP and not from CP-DNA interactions. Furthermore, the encapsulated samples were treated with DNase I, which cleaves the strand randomly, in that way releasing the dyes from the DNA strand. A minimal change in the energy transfer is observed in this experiment, indicating

that the VLP capsid protects the encapsulated DNA against nuclease, which has previously been shown for encapsulated RNA [29].

Conclusion

This work shows the successful formation of CCMV VLPs around short DNA-dye constructs, containing a mixture of both double- and single-stranded DNA. Based on the size, the resulting particle sizes correspond to $T = 1$ or pseudo $T = 2$ icosahedral symmetry. The encapsulation of this DNA-photonic wire in the VLP resulted in an almost eight-fold increase in FRET efficiency of one-step FRET systems and a 16-fold increase for a two-step energy transfer. Furthermore, decomposition of VLP by Trypsin digestion yields an energy transfer signal similar in intensity as the signal before encapsulation, suggesting that FRET must be induced by the capsid formation and not by protein-DNA interactions. Consequently, the FRET system can be used as a probe to study the assembly and disassembly of viruses.

Overall, the system we developed is a probe for virus disassembly and cargo release, which possibly can be applied to other viruses as well. This can be especially useful in virus life-cycle analysis in cells. Also, it can be used as an FRET-based sensor during force-based measurements on a virus to indicate cargo leaching or virus breakdown [40]. Alternatively, a fully double-stranded DNA photonic wire could be used as a template for encapsulations, which would result in rods enveloped in protective virus coats [19, 41]. This might find application in light harvesting and energy transfer. Future work of our group will focus on using the DNA hybrids to load different cargos, such as drugs or proteins, in specific ratios inside a VLP for intracellular delivery [41, 42].

Acknowledgments

We acknowledge financial support from the European Research Council (ERC Consolidator Grant, Protocage). GS acknowledges the Australian Federal Government for an Australian Postgraduate Award (APA).

ORCID iDs

Nico J Overeem  <https://orcid.org/0000-0003-0171-3435>

Jeroen J L M Cornelissen  <https://orcid.org/0000-0002-9728-5043>

References

- [1] Lilley D M J 2000 Structures of helical junctions in nucleic acids *Q. Rev. Biophys.* **33** 109–59
- [2] Medintz I L *et al* 2006 Proteolytic activity monitored by fluorescence resonance energy transfer through quantum-dot-peptide conjugates *Nat. Mater.* **5** 581–9
- [3] Pollok B A and Heim R 1999 Using GFP in FRET-based applications *Trends Cell Biol.* **9** 57–60

- [4] Sekar R B and Periasamy A 2003 Fluorescence resonance energy transfer (FRET) microscopy imaging of live cell protein localizations *J. Cell Biol.* **160** 629–33
- [5] Buckhout-White S *et al* 2014 Assembling programmable FRET-based photonic networks using designer DNA scaffolds *Nat. Commun.* **5** 5615
- [6] Spillmann C M *et al* 2014 Extending FRET cascades on linear DNA photonic wires *Chem. Commun.* **50** 7246–9
- [7] Matczyszyn K and Olesiak-Banska J 2012 DNA as scaffolding for nanophotonic structures *J. Nanophotonics* **6** 064505
- [8] Dirk B S, Van Nynatten L R and Dikeakos J D 2016 Where in the cell are you? Probing HIV-1 host interactions through advanced imaging techniques *Viruses* **8** 288
- [9] Müller B, Anders M and Reinstein J 2014 *In vitro* analysis of human immunodeficiency virus particle dissociation: gag proteolytic processing influences dissociation kinetics *PLoS One* **9** e99504
- [10] Martin-Fernandez M *et al* 2004 Adenovirus type-5 entry and disassembly followed in living cells by FRET, fluorescence anisotropy, and FLIM *Biophys. J.* **87** 1316–27
- [11] Jensen E C 2012 Use of fluorescent probes: their effect on cell biology and limitations *Anatomical Rec.* **295** 2031–6
- [12] Ma Y, Nolte R J M and Cornelissen J J L M 2012 Virus-based nanocarriers for drug delivery *Adv. Drug Deliv. Rev.* **64** 811–25
- [13] Aniahyei S E *et al* 2009 Synergistic effects of mutations and nanoparticle templating in the self-assembly of cowpea chlorotic mottle virus capsids *Nano Lett.* **9** 393–8
- [14] Fox J M *et al* 1998 Comparison of the native CCMV virion with *in vitro* assembled CCMV virions by cryoelectron microscopy and image reconstruction *Virology* **244** 212–8
- [15] Sikkema F D *et al* 2007 Monodisperse polymer-virus hybrid nanoparticles *Org. Biomol. Chem.* **5** 54–7
- [16] Kwak M *et al* 2010 Virus-like particles templated by DNA micelles: a general method for loading virus nanocarriers *J. Am. Chem. Soc.* **132** 7834–5
- [17] Hu Y *et al* 2008 Packaging of a polymer by a viral capsid: the interplay between polymer length and capsid size *Biophys. J.* **94** 1428–36
- [18] Liu A *et al* 2016 Protein cages as containers for gold nanoparticles *J. Phys. Chem. B* **120** 6352–7
- [19] Mukherjee S *et al* 2006 Redirecting the coat protein of a spherical virus to assemble into tubular nanostructures *J. Am. Chem. Soc.* **128** 2538–9
- [20] Mikkilä J *et al* 2014 Virus-encapsulated DNA origami nanostructures for cellular delivery *Nano Lett.* **14** 2196–200
- [21] Garmann R F *et al* 2016 Physical principles in the self-assembly of a simple spherical virus *Acc. Chem. Res.* **49** 48–55
- [22] Brinkers S *et al* 2009 The persistence length of double stranded DNA determined using dark field tethered particle motion *J. Chem. Phys.* **130** 21505
- [23] Rechendorff K *et al* 2009 Persistence length and scaling properties of single-stranded DNA adsorbed on modified graphite *J. Chem. Phys.* **131** 095103
- [24] Brasch M *et al* 2017 Assembling enzymatic cascade pathways inside virus-based nanocages using dual-tasking nucleic acid tags *J. Am. Chem. Soc.* **139** 1512–9
- [25] Gunnarsson G H *et al* 2006 Two-dimensional strandness-dependent electrophoresis *Nat. Protocols* **1** 3011–8
- [26] Cavaluzzi M J and Borer P N 2004 Revised UV extinction coefficients for nucleoside-5'-monophosphates and unpaired DNA and RNA *Nucl. Acids Res.* **32** e13
- [27] Verduin B J M 1974 The preparation of CCMV-protein in connection with its association into a spherical particle *FEBS Lett.* **45** 50–4
- [28] Comellas-Aragones M *et al* 2007 A virus-based single-enzyme nanoreactor *Nat. Nano* **2** 635–9
- [29] Cadena-Nava R D *et al* 2012 Self-assembly of viral capsid protein and RNA molecules of different sizes: requirement for a specific high protein/RNA mass: ratio *J. Virol.* **86** 3318–26
- [30] Fábíán A *et al* 2013 TripleFRET measurements in flow cytometry *Cytometry A* **83A** 375–85
- [31] Caspar D L and Klug A 1962 Physical principles in the construction of regular viruses *Cold Spring Harbor Symp. Quant. Biol.* **27** 1–24
- [32] Lavelle L *et al* 2009 Phase diagram of self-assembled viral capsid protein polymorphs *J. Phys. Chem. B* **113** 3813–9
- [33] Watrob H M, Pan C P and Barkley M D 2003 Two-step FRET as a structural tool *J. Am. Chem. Soc.* **125** 7336–43
- [34] Wang J C 1979 Helical repeat of DNA in solution *Proc. Natl. Acad. Sci. USA* **76** 200–3
- [35] Chi Q, Wang G and Jiang J 2013 The persistence length and length per base of single-stranded DNA obtained from fluorescence correlation spectroscopy measurements using mean field theory *Physica A* **392** 1072–9
- [36] Murphy M C *et al* 2004 Probing single-stranded DNA conformational flexibility using fluorescence spectroscopy *Biophys. J.* **86** 2530–7
- [37] Ramachandran R *et al* 2008 Persistence length of short-chain branched polyethylene *Macromolecules* **41** 9802–96
- [38] Bayer T S *et al* 2005 Arginine-rich motifs present multiple interfaces for specific binding by RNA *RNA* **11** 1848–57
- [39] Zlotnick A, Porterfield J Z and Wang J C Y 2013 To build a virus on a nucleic acid substrate *Biophys. J.* **104** 1595–604
- [40] Harke B *et al* 2012 A novel nanoscopic tool by combining AFM with STED microscopy *Opt. Nanoscopy* **1** 1–6
- [41] Azizgolshani O *et al* 2013 Reconstituted plant viral capsids can release genes to mammalian cells *Virology* **441** 12–7
- [42] Yildiz I *et al* 2013 Infusion of imaging and therapeutic molecules into the plant virus-based carrier cowpea mosaic virus: cargo-loading and delivery *J. Control. Release* **172** 568–78